MATERIALS SCIENCE

Bioinspired electrospun dECM scaffolds guide cell growth and control the formation of myotubes

Mollie M. Smoak, Katie J. Hogan, K. Jane Grande-Allen, Antonios G. Mikos*

While skeletal muscle has a high capacity for endogenous repair in acute injuries, volumetric muscle loss can leave long-lasting or permanent structural and functional deficits to the injured muscle and surrounding tissues. With clinical treatments failing to repair lost tissue, there is a great need for a tissue-engineered therapy to promote skeletal muscle regeneration. In this study, we aim to assess the potential for electrospun decellularized skeletal muscle extracellular matrix (dECM) with tunable physicochemical properties to control mouse myoblast growth and myotube formation. The material properties as well as cell behavior – growth and differentiation – were assessed in response to modulation of crosslinking and scaffold architecture. The fabrication of a bioactive dECM-based system with tunable physicochemical properties that can control myotube formation has several applications in skeletal muscle engineering and may bring the field one step closer to developing a therapy to address these unmet clinical needs.

INTRODUCTION

Skeletal muscle comprises more than 40% of the average adult body by mass and is responsible for support and movement of the skeletal system. Strains and contusions as a result of exercise and lacerations due to surgical operation are common skeletal muscle injuries. Thankfully, skeletal muscle has a high capacity for self-repair in acute injuries such as these. However, volumetric muscle loss (VML) due to high-intensity sports injuries, battlefield trauma, and tumor ablation often results in permanent loss of muscle structure and function (*1*, *2*). Due to the nature of VML injuries, the surrounding tissues and underlying musculoskeletal system also suffer loss of function, creating a compound effect. Recent reports attribute musculoskeletal injuries to more than 50% of all Department of Defense disabilities and approximately 35 to 55% of all sports-induced injuries, constituting approximately 4.5 million reconstructive surgeries per year (*3*).

With clinical treatments (often autografts) leading to limited structural restoration and little to no functional repair of skeletal muscle lost in VML injuries (*4*–*6*), there is a great need for a tissue-engineered therapy for the regeneration of skeletal muscle. In recent years, decellularized extracellular matrix (dECM) products have become an attractive platform for several tissue engineering applications because of the retention of tissue-specific biochemical cues. Tissues, including dermis, small intestinal submucosa, and bladder, have been used in skeletal muscle applications with varying degrees of success (*5*, *7*, *8*). Overall, it has been shown that the biochemical signals retained during decellularization promote cell integration, growth, and myogenic differentiation. In addition, recent studies have demonstrated increased angiogenic and neurogenic effects with dECM treatments (*5*, *7*). It is well documented that cross-talk exists between these pathways and myogenesis, indicating that all three pathways may be necessary to grow functional skeletal muscle (*9*–*11*). While dECM has many advantages, there is limited control over its physicochemical properties, and it is often difficult to scale up to clinically relevant shapes and sizes. Therefore, scaffold fabrication techniques, such as electrospinning and bioprinting, have been leveraged to provide tunability of dECM scaffolds (*12*).

Department of Bioengineering, Rice University, Houston, TX 77030, USA.
*Corresponding author. Email: mikos@rice.edu

Electrospinning is a high-throughput technique that produces high-porosity scaffolds with control over fiber orientation. Because of the highly aligned nature of skeletal muscle that contributes to the function of the tissue, recapitulating precise architecture is an important material property for potential skeletal muscle therapies (*12*). Electrospun synthetic and hybrid polymers have been used for skeletal muscle engineering to create biomaterials that provide substrate architecture and mechanical properties to support myogenic differentiation (*13*–*18*). Our laboratory has recently developed a method of electrospinning skeletal muscle dECM without the need for a carrier polymer (*19*). Unlike other natural polymers, such as collagen and gelatin, electrospun dECM can be retained within collagenase-supplemented media for up to 4 weeks without the addition of a cross-linking agent. Stability without cross-linking provides added versatility to the biomaterial because many studies have shown that access to free amines improves cell adhesion in vitro (*20*–*22*) and influences regeneration in vivo (*23*). In addition, we demonstrated that mechanical properties and degradation kinetics could be further controlled through the modulation of scaffold architecture and the incorporation of a cross-linking agent. Along with the unique physicochemical properties of the electrospun dECM, the decellularization process used for our system was able to remove DNA below the standard 50 ng/mg while retaining relevant proteins and sulfated glycosaminoglycans, which are important for the retention of growth factors (*24*, *25*).

Inspired by these results, this study aims to further demonstrate the tunability of electrospun dECM and assess its bioactivity in vitro. To our knowledge, this is the first study to investigate a highly tunable electrospun scaffold completely derived from skeletal muscle dECM within an in vitro myogenic model. The relationship between dECM cross-linking density and exposure to glutaraldehyde (GA) vapor was assessed and used to inform the study design. Furthermore, the relationship between mandrel speed and dECM fiber alignment was assessed to develop scaffolds with extreme and intermediate degrees of alignment. The effects of cross-linking density and fiber alignment on fiber swelling, bulk swelling, and bulk tensile mechanical properties were investigated. The dry fiber size was kept consistent between groups to isolate the effects of these parameters. Upon fabricating dECM scaffolds with varying degrees of fiber

alignment and cross-linking and measuring their effects on material properties, the potential for dECM scaffolds to support cell attachment, growth, and myogenic differentiation was assessed. Myotube length, width, alignment, and fusion index were measured to explore the influence of varying degrees of cross-linking and fiber alignment on cell behavior. Last, the ability for cells to remodel the dECM substrate was measured through changes in scaffold diameter for all culture points.

RESULTS

Experimental design

To investigate the cell response to electrospun dECM properties, we chose to modulate fiber orientation and the degree of cross-linking of electrospun dECM scaffolds. A full factorial design was used to fabricate nine groups of electrospun dECM scaffolds. The degree of fiber alignment will be noted as RO (randomly oriented), AO (aligned orientation) 1000 (mandrel speed set to 1000 rpm), and AO 3000 (mandrel speed set to 3000 rpm). The degree of cross-linking will be noted by the addition of an "X" followed by either 30 or 24 for 30 min or 24 hours in GA vapor, respectively. All group abbreviations and fabrication descriptors are listed in Table 1.

Electrospinning dECM

Two electrospinning setups were used to fabricate 3° of fiber alignment. For the least aligned group (RO), dECM fibers were collected onto a stationary plate (fig. S1A). Electrospinning parameters were chosen such that the highest flow rate that produced uniform, single micrometer-scale fibers was selected. For the most aligned group (AO 3000), dECM fibers were collected onto a rotating collector (fig. S1B). Electrospinning parameters were chosen to produce the most aligned fibers that did not substantially differ in fiber diameter from RO fibers and did not exhibit splitting due to tension. Past 3000 rpm (8.38 m/s), the flow rate needed to produce intact fibers created fibers that were significantly larger than the RO group. For the intermediate degree of fiber alignment, a mandrel speed that produced roughly 50% fiber alignment was chosen (1000 rpm).

Evaluation of degree of fiber alignment

The degree of fiber alignment for each of the three groups (RO, AO 1000, and AO 3000) was assessed through confocal imaging and analysis through the National Institutes of Health (NIH) ImageJ (n = 5). dECM was incubated with fluorescein before electrospinning to allow for confocal imaging. As the speed of the collector increased, there was a qualitative (Fig. 1, A to C) and quantitative (Fig. 1D) increase in the degree of fiber alignment. Under stationary conditions, the RO fibers produced a nearly flat distribution curve, indicating the lack of alignment. The AO 3000 group contained 70.7 ± 3.7% of fibers oriented within 10° of the origin. This was a significant increase compared to the AO 1000 group (42.3 ± 2.6%), which was significantly higher than the RO group (20.5 ± 5%).

Table 1. dECM abbreviations and fabrication descriptions for all groups used in this study.

Abbreviation	Collector speed	GA vapor exposure time
RO	0 rpm	0 min
ROX 30	0 rpm	30 min
ROX 24	0 rpm	24 hours
AO 1000	1000 rpm	0 min
AOX 1000 30	1000 rpm	30 min
AOX 1000 24	1000 rpm	24 hours
AO 3000	3000 rpm	0 min
AOX 3000 30	3000 rpm	30 min
AOX 3000 24	3000 rpm	24 hours

Evaluation of degree of cross-linking

Similar to many other natural electrospun meshes, dECM was cross-linked by exposure to GA vapor. As the scaffolds become more cross-linked, fewer free amines are present. As shown in Fig. 2A, the degree of cross-linking of dECM scaffolds can be controlled by adjusting the amount of time that dECM samples are exposed to GA vapor. The degree of cross-linking was calculated by first measuring the concentration of free amines via a ninhydrin assay (n = 4). All groups were normalized to uncross-linked dECM (0 min). As shown previously, electrospun dECM scaffolds can be used without any cross-linking agent (*19*). The relationship between GA exposure time and amine sequestration was not linear. After only 10 min, approximately 38% of amines were bound. After 24 hours in GA vapor, dECM scaffolds were 100% cross-linked. To provide an intermediate group, dECM was cross-linked in GA vapor for 30 min, which produced samples that were 70.4 ± 4.7% cross-linked.

Evaluation of fiber swelling

The swelling behavior of all acellular dECM groups was evaluated via confocal imaging paired with analysis through NIH ImageJ (n = 5). As stated above, one of the goals in optimizing electrospinning parameters for different groups was to produce dry fibers of similar size to isolate the effects of cross-linking and fiber alignment on material properties and cell behavior. As shown in Fig. 2B, there was no significant difference in the dry fibers between any of the groups. For the random fibers, there was a significant increase in fiber diameter in the swollen RO (5.0 ± 1.8 μm) and ROX 30 (4.7 ± 1.1 μm) groups compared to the dry RO fibers (3.6 ± 1.3 μm) and no significant change in the ROX 24 group (3.7 ± 1.1 μm). This demonstrates that increased cross-linking results in decreased swelling. In the aligned groups (AO 1000 and AO 3000), there was no observable change in fiber diameter between the dry and swollen fibers regardless of the degree of cross-linking. This suggests that alignment may also limit the swelling of dECM fibers.

Evaluation of bulk scaffold swelling

In addition to assessing single-fiber swelling behavior, bulk scaffold swelling was also measured. Qualitatively, it was observed that swollen RO scaffold groups resembled the original circular scaffolds created through the use of a biopsy punch. However, aligned scaffolds tended to become more elliptical in shape when swollen. This phenomenon was further measured (n = 5) and reported as the minor axis length (Fig. 2C), the major axis length (Fig. 2D), and the aspect ratio (Fig. 2E). The aspect ratio (Fig. 2E) is defined here as the major elliptical axis over the minor elliptical axis. As observed qualitatively, when the RO scaffold groups swelled, they retained an aspect ratio close to 1, which represents a perfect circle. The swollen AO 1000 (1.17 ± 0.02) and AOX 1000 30 (1.19 ± 0.03) groups had a

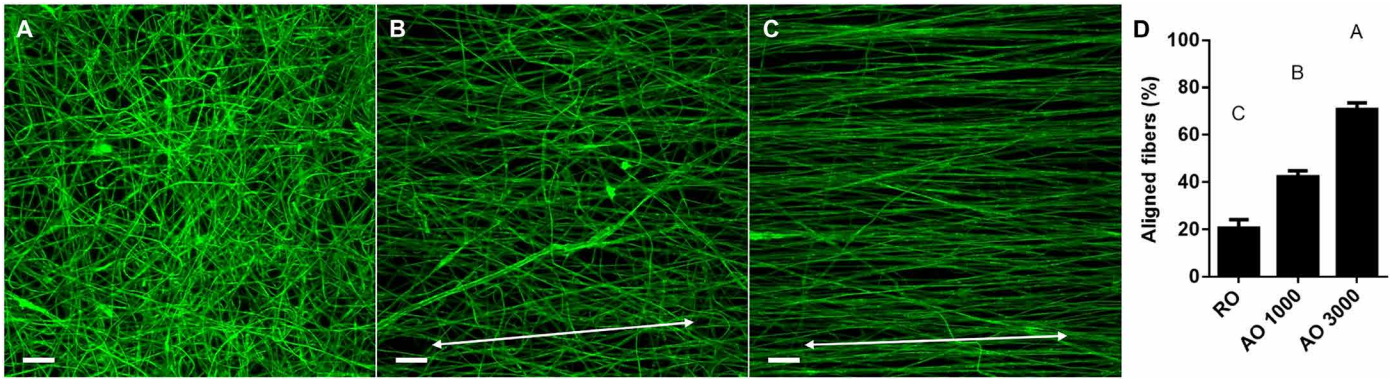

Fig. 1. Tunable electrospun dECM fibers. (**A**) Confocal images of random (RO) fibers, (**B**) aligned fibers fabricated on a collector rotating at 1000 rpm (AO 1000), and (**C**) aligned fibers fabricated on a collector rotating at 3000 rpm (AO 3000). (**D**) Orientation graph of electrospun fibers aligned within 10° of the origin expressed as a percentage of all fibers. Scale bar represents 50 μm and is the same across images. The white double-headed arrow represents the direction of fiber alignment. Values represent means ± SD ($n = 5$). Bars that share letters are not significantly different. Conversely, bars that do not share a letter are significantly different ($P < 0.05$).

significantly higher aspect ratio than the AOX 1000 24 group (1.03 ± 0.01), which did not significantly differ from the RO groups (1.00 ± 0.01). A similar trend was observed in the swollen AO 3000 groups. Swollen AO 3000 (1.24 ± 0.02) and AOX 3000 30 (1.26 ± 0.03) groups had the highest aspect ratio of all the groups, while AOX 3000 24 did not significantly differ from AOX 1000 24. For the aligned groups, the minor axis corresponds to the direction of fiber alignment (Fig. 2C and fig. S2), while the major elliptical axis lies perpendicular to the fiber direction (Fig. 2D and fig. S2). To understand these trends, it is important to examine the swelling behavior of each axis. As the uncross-linked groups swelled, their scaffold diameter decreased. A similar change was observed along both axes in the RO scaffolds. A greater decrease was measured along the fiber direction in the AO 1000 and AO 3000 groups. The length of the aligned fibers also shortened, creating an elliptical shape and increasing the aspect ratio. A similar trend was observed in the AOX 1000 30 and AOX 3000 30 groups. Cross-linking for 24 hours appeared to retain the original structure. There were no significant differences between the major axis in these groups, regardless of fiber alignment. While there was a decrease in minor axis length as fiber alignment increased, the 24-hour groups were retained to a higher degree than the uncross-linked and 30-min cross-linked scaffolds within each alignment group. These results suggest that cross-linking is the main factor contributing to bulk scaffold swelling, but the degree of alignment affects the symmetry of the swollen scaffolds.

Mechanical testing of dECM scaffolds

The final material property assessed was the influence of fiber alignment and cross-linking density on bulk tensile mechanical properties (Fig. 2F). In a hydrated mechanical testing chamber, swollen dECM scaffolds ($n = 3$) were pulled to an extension of 12 mm. As fibers became more aligned, the bulk tensile modulus increased. Similarly, as the cross-linking density increased, bulk tensile moduli increased within each alignment group, with the most observable impacts observed in the AO 3000 group. AOX 3000 24 had the highest tensile modulus (1101 ± 128 kPa), followed by AOX 3000 30 (648 ± 64 kPa), and AO 3000 (494 ± 51 kPa). While not significantly different when analyzed with the other groups, the AO 1000 group had a higher tensile modulus (111 ± 9 kPa) than the RO group (42 ± 8 kPa), further supporting the hypothesis that tensile mechanical properties increase with increased degree of fiber alignment. The same trend was observed within alignment groups as cross-linking density increased, with the 24-hour cross-linking groups having a tensile modulus approximately double that of the uncross-linked group within each alignment.

C2C12 growth on dECM scaffolds

Figure 3 is a schematic outlining the dECM scaffold seeding and culture conditions used for this study. After attaching to dECM scaffolds overnight in a rotating system, C2C12 myoblasts were cultured in stationary plates for 4 days in growth media to allow proliferation and cell spreading to take place. After 2 and 4 days in growth media, cell-laden scaffolds were fixed, and nuclei and actin staining was performed ($n = 6$). With dynamic seeding, cells attached to both sides of the scaffold but only proliferated and differentiated on the top side once in static culture. To isolate the top side for analysis, cell count and confluency were measured through imaging. As shown in Fig. 4J, the AOX 1000 24 and AOX 3000 24 groups contained fewer cells at days 2 and 4 compared with their less cross-linked counterparts. There was also a significant increase in cell number in AO 1000 and AO 3000 scaffolds compared to RO scaffolds at day 2, indicating that more structured fiber alignment may help to promote cell adhesion and early growth. There was no significant increase in nuclei count between days 2 and 4 within each group, but actin staining did reveal a qualitative increase in cell confluency. The scaffolds cross-linked for 24 hours tended to have lower nuclei counts than their counterparts. This trend was further supported through confocal imaging of actin cytoskeletons. By day 4, all 30-min cross-linking groups (Fig. 4, D to F) contained a confluent layer of cells to the extent that cells began to grow on top of one another. This was also observed in the AO 1000 and AO 3000 groups and, to a lesser extent, in RO samples (Fig. 4, A to C). In the 24-hour cross-linking groups, however, cells were less confluent across alignments.

Myotube formation on dECM scaffolds

Myotube formation was assessed for all groups after 7 days of culture in induction media. Myotube formation was observed in all uncross-linked and intermediate cross-linking groups. No myotube formation was observed in the 24-hour cross-linked groups regardless

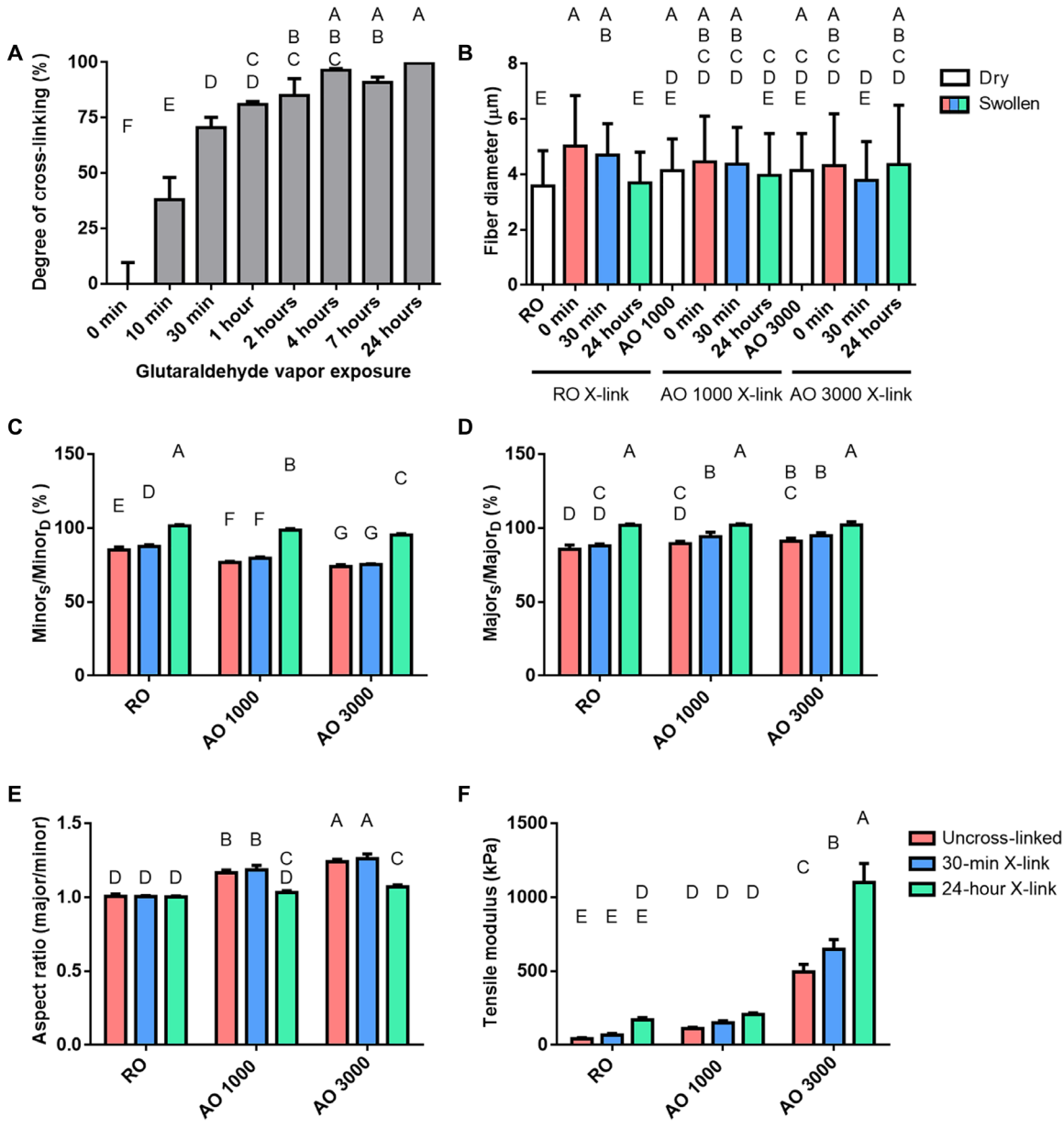

Fig. 2. Material characterization of tunable dECM scaffolds. (**A**) The degree of cross-linking of electrospun dECM was determined via ninhydrin assay. dECM scaffolds were exposed to GA vapor for variable amounts of time (10 min to 24 hours) and normalized to uncross-linked samples (0 min). (**B**) The diameter of dECM fibers dry and after swelling in PBS for 24 hours was measured. The bulk dECM scaffold swelling behavior expressed as (**C**) the elliptical axis along the fibers (swollen minor/dry minor), (**D**) the elliptical axis perpendicular to the fiber direction (swollen major/dry major), (**E**) and the aspect ratio ($Major_S/Minor_S$) of swollen scaffolds was measured ($Major_S$, swollen major axis; $Minor_S$, swollen minor axis; $Major_D$, dry major axis; $Minor_D$, dry minor axis). (**F**) The tensile mechanical properties of swollen dECM scaffolds tested via a uniaxial testing system under aqueous conditions. Values represent means ± SD [$n = 4$ (A), $n = 5$ (B to E), and $n = 3$ (F)]. Bars that share letters are not significantly different. Conversely, bars that do not share a letter are significantly different ($P < 0.05$).

of alignment. Immunostaining for a myogenic marker was performed to isolate differentiated myotubes. Desmin-positive myotubes were imaged along with actin and nuclei via confocal microscopy ($n = 9$). Once isolated, alignment, fusion index, length, and width of desmin-positive myotubes were measured. Figure 5 shows representative myotube images along with their orientation graphs. AOX 3000 30 scaffolds produced significantly more aligned myotubes than any of the other groups (88.5 ± 8.8% within 10°) (Fig. 6A). The second most aligned groups were produced by AO 3000 scaffolds (66.0 ± 16.1%) followed by AOX 1000 30 (51.2 ± 14.6%). There was no significant difference in myotube alignment in the RO, ROX 30, and AO 1000 groups.

When analyzing fusion index (the number of nuclei per myotube), there was a very large distribution in the size of the myotubes assessed. Therefore, there was no significant difference observed in fusion index between groups (Fig. 6B). The shape of the myotubes is also an important metric, as myofibers tend to be elongated. The longest myotubes were produced by the AO 3000 and AOX 3000 30

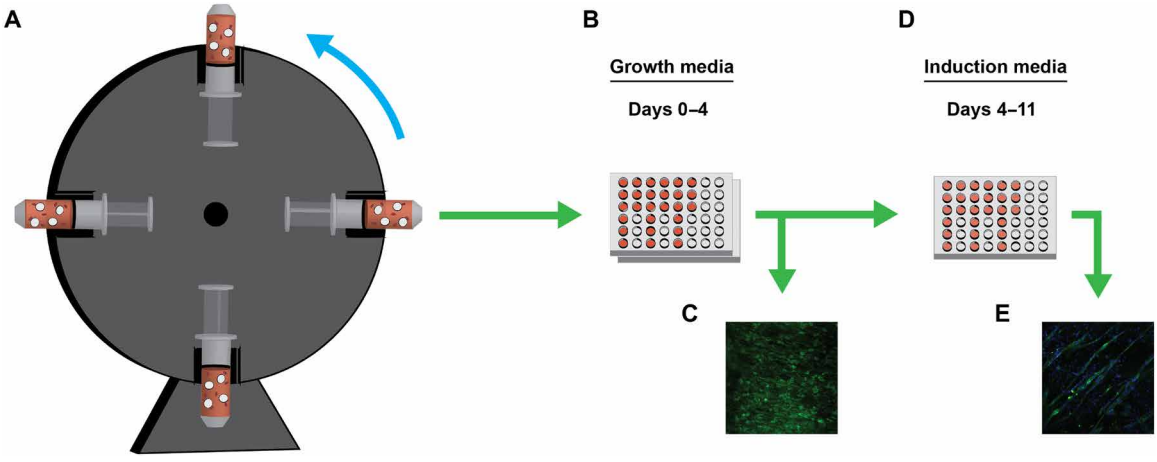

Fig. 3. In vitro setup and analysis of myogenic behavior. (**A**) C2C12 myoblasts were allowed to attach to dECM scaffolds while being incubated overnight on a rotating system. (**B**) After seeding, cell-laden scaffolds were collected and cultured in stationary plates in growth media for 4 days. (**C**) At 2 and 4 days in growth media, cell growth was assessed. (**D**) After 4 days, growth media was swapped for induction media. Cells were then allowed to differentiate for 7 days. (**E**) Myotube formation was then assessed on cell-laden scaffolds.

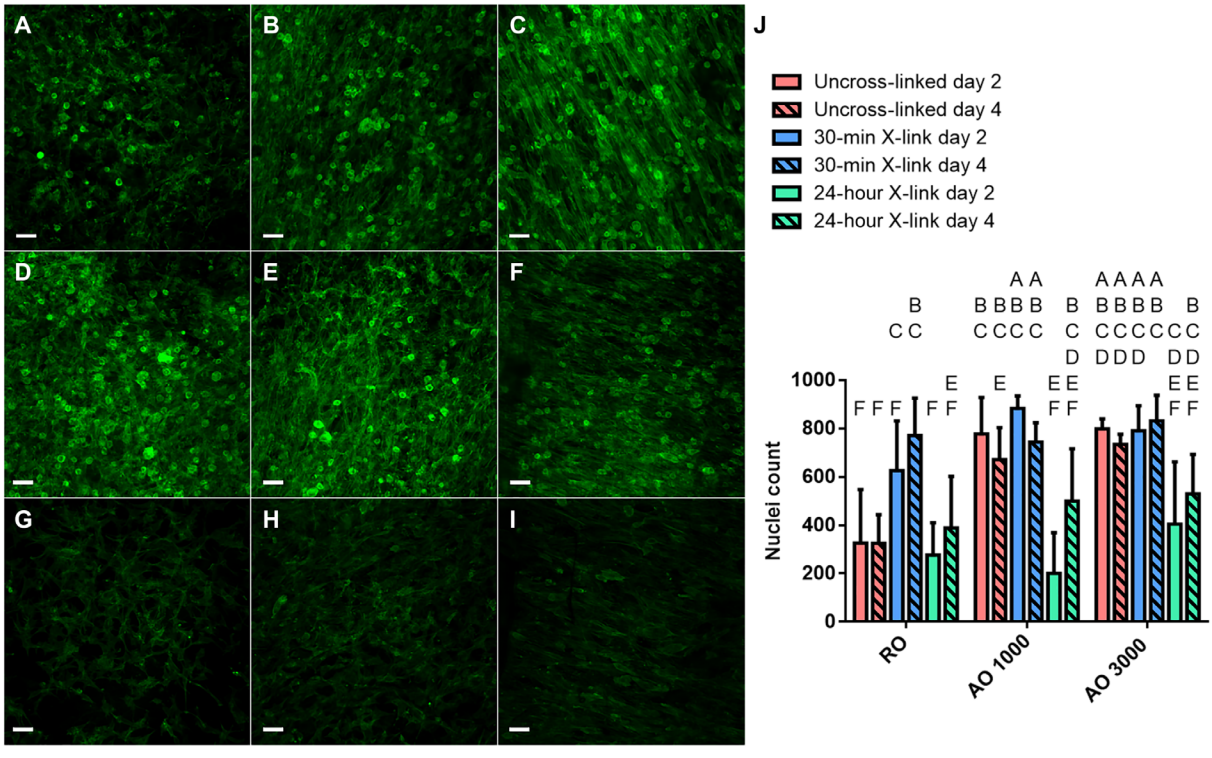

Fig. 4. C2C12 growth on dECM scaffolds. Cell growth was assessed after 2 and 4 days in growth media through staining of the actin cytoskeleton. (**A** to **I**) Representative confocal images of cell-laden dECM constructs after 4 days of growth are shown. Immunofluorescence staining of actin is shown in green. Scale bar represents 50 μm and is the same across images. (**J**) Cell number was assessed on days 2 and 4 of culture in growth media. Values represent means ± SD ($n = 6$). Bars that share letters are not significantly different. Conversely, bars that do not share a letter are significantly different ($P < 0.05$).

groups (179.7 ± 63.2 and 199.0 ± 63.5 μm, respectively) (Fig. 6C). The shortest myotubes were produced on RO scaffolds (126.3 ± 43.2 μm). The inverse trend was observed when assessing myotube width (Fig. 6D). The widest myotubes were produced in the RO, ROX 30, and AO 1000 groups (27.5 ± 4.2, 29.4 ± 4.5, and 26.0 ± 9.2 μm, respectively). AOX 1000 30, AO 3000, and AOX 3000 30 groups were significantly narrower. The number of myotubes formed on each scaffold was also measured (Fig. 6E). The 30-min cross-linked groups tended to support more myotube growth than their uncross-linked counterparts.

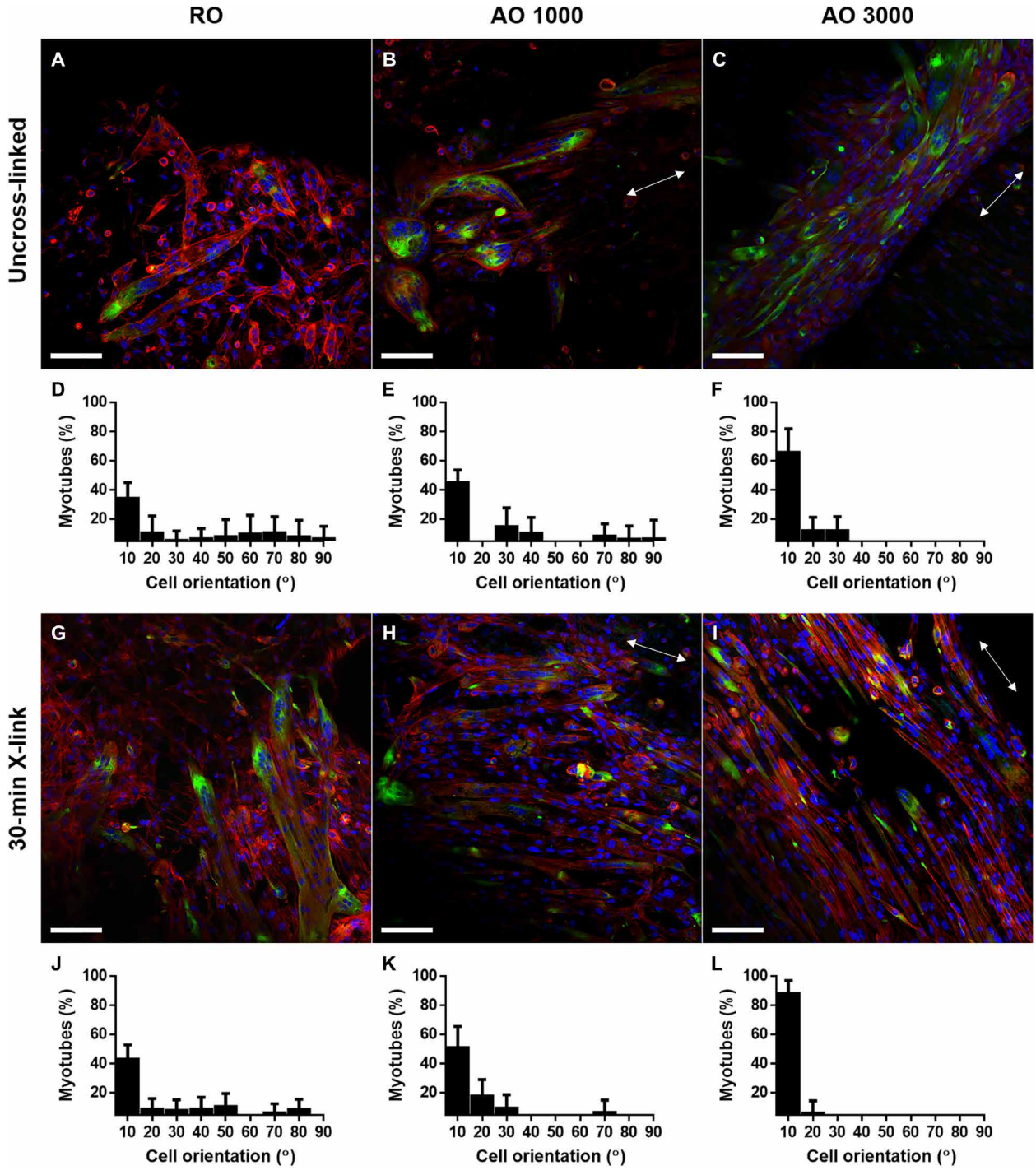

Fig. 5. Alignment of myotubes formed on dECM scaffolds. Immunofluorescence staining of myotube formation [desmin (green), actin (red), and nuclei (blue)] was captured via confocal microscopy. (**A** to **C** and **G** to **I**) Representative images of myotube formation and (**D** to **F** and **J** to **L**) the orientation graphs of myotubes grown on cell-laden dECM constructs after 7 days in induction media are shown. Scale bar represents 100 μm and is the same across images. The white double-headed arrow represents the direction of myotube alignment. Values represent means ± SD ($n = 9$).

In vitro scaffold degradation

The diameter of cell-laden dECM constructs was measured directly before seeding and at each of the culture time points to assess the ability for cells to remodel the dECM substrate (Fig. 6F). There was no substantial change observed in the 24-hour cross-linked groups across time points. After 11 days in culture, 99.1, 98.5, and 99.6% of the original scaffold diameter remained in the ROX 24, AOX 1000 24, and AOX 3000 24 scaffolds, respectively. The greatest degradation was observed in the 30-min cross-linked groups. By day 11 in culture, 86.8, 65.5, and 67.2% of the original scaffold diameter

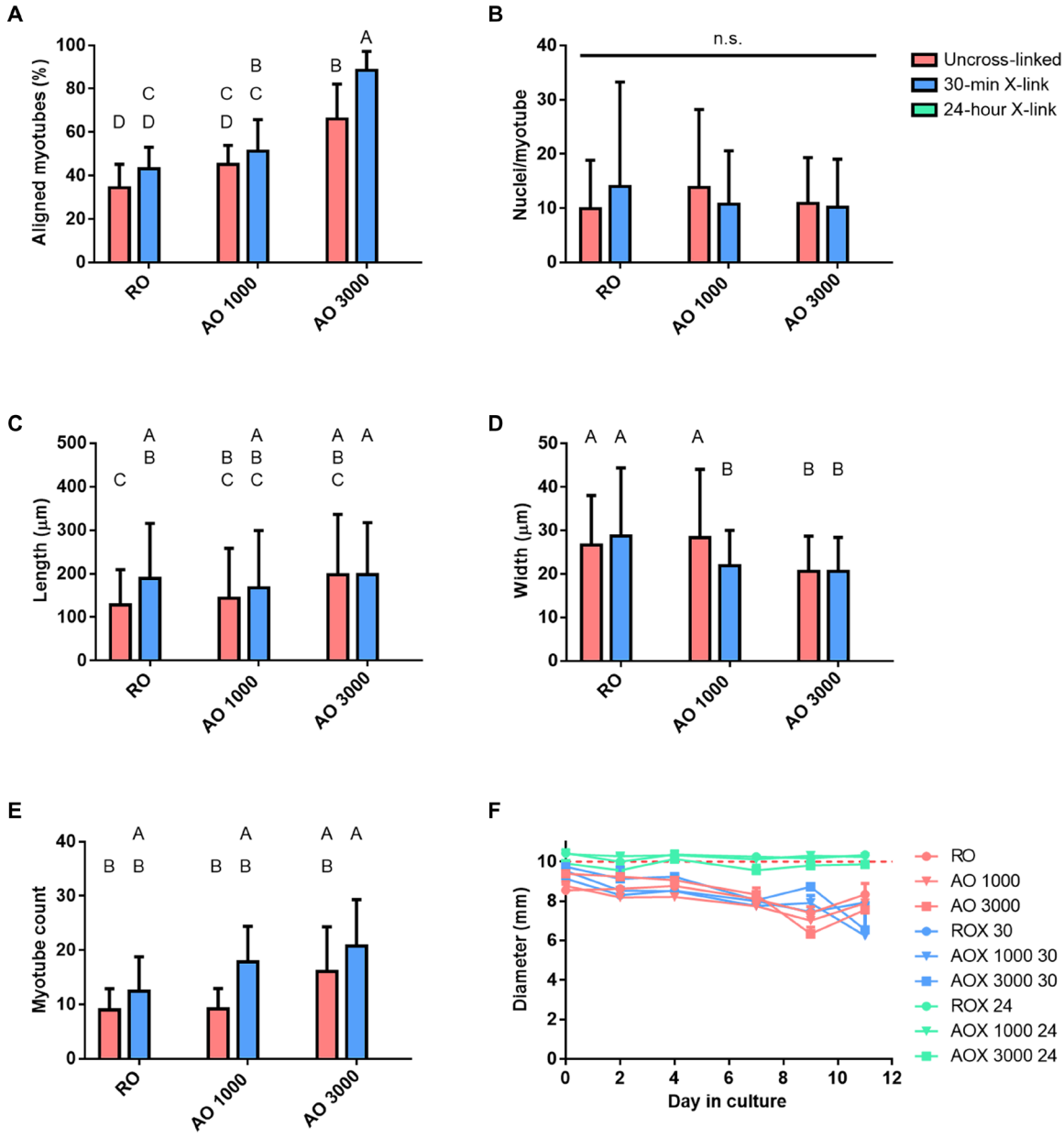

Fig. 6. Analysis of myotube formation on dECM scaffolds. Myotube formation was assessed after 7 days of culture in induction media. (**A**) Myotubes aligned within 10° of the origin expressed as a percentage of all myotubes, (**B**) fusion index (nuclei per myotube), (**C**) myotube length, and (**D**) myotube width were assessed from confocal images. (**E**) Myotubes per image were counted and reported for each group. (**F**) In vitro scaffold degradation was assessed throughout the 11 days that cell-laden scaffolds were cultured. Samples were cultured in growth media during days 0 to 4 and then switched to induction media during days 4 to 11. Values represent means ± SD [$n = 9$ (A to E) and $n = 3$ (F)]. Bars that share letters are not significantly different. Conversely, bars that do not share a letter are significantly different ($P < 0.05$). n.s. indicates no significant difference between all groups ($P < 0.05$).

remained in the ROX 30, AOX 1000 30, and AOX 3000 30 groups, respectively. Both the cross-linking density and degree of alignment seemed to affect the degradation. Overall, the greatest retention was observed in the 24-hour cross-linked groups, followed by the uncross-linked groups, and then the 30-min cross-linked groups with the greatest percent degradation. Fiber alignment also affected remodeling, with the greatest loss observed in the 1000-rpm group followed by the 3000-rpm group, and lastly the random orientation for the uncross-linked and 30-min cross-linked groups. In most of the groups, there was a burst of degradation observed at day 2 and another burst observed during the differentiation phase of culture (days 4 to 11).

DISCUSSION

Over the course of this study, we have demonstrated the tunability and bioactivity of electrospun skeletal muscle dECM. We have applied a full factorial study design to fabricate nine groups of varying

degrees of fiber alignment and cross-linking density. After characterizing the effects of these parameters on material properties, we assessed their potential to guide myotube formation in vitro. While previous studies have shown an increased cell response from electrospun scaffolds with the addition of dECM components (*17*, *26*), this is the first study that we are aware of that investigates a highly tunable scaffold completely derived from skeletal muscle dECM within an in vitro myogenic model. Characterization of the electrospun dECM revealed that protein and sulfated glycosaminoglycans were retained through processing (*19*), but the bioactivity of the matrix and the extent to which the material properties could be modulated had not been previously investigated.

By adjusting the collector speed and the length of time dECM was exposed to GA vapor, the degree of fiber alignment and the cross-linking density were tuned, respectively. Increasing the mandrel to 3000 rpm was the upper limit for the collector before tears were observed due to the tension on the dECM fibers. Native skeletal muscle has highly aligned architecture, which we aimed to replicate in this group. An intermediate fiber alignment and a random fiber dispersion were also selected (Fig. 1) to study the effects of fiber orientation on material properties and cell behavior. To isolate this variable, electrospinning parameters were tuned to produce fibers of statistically similar size in all three orientations (Fig. 2B). The degree of cross-linking was also selected as a variable for this study because cross-linking has been shown to affect key material properties, such as material stiffness and degradation kinetics (*19*, *27*), as well as cell attachment through binding of free amines (*20*–*22*). The rate of cross-linking of electrospun dECM was very rapid (Fig. 2A) compared to other studies reported for natural polymers (*28*). Uncross-linked and fully cross-linked (24-hour) samples were used as extremes, and the 30-min GA exposure (~70% cross-linked) was used as an intermediate.

As shown in Fig. 2C, degree of alignment affects the bulk swelling behavior of dECM scaffolds. As fiber alignment increases, the aspect ratio increases. As aligned scaffolds swell, there is a slight decrease in porosity (*19*), drawing the fibers closer together and causing a decrease in the bulk axis diameter perpendicular to the fiber direction. The length of the aligned fibers shortens more substantially, creating an elliptical shape and increasing the aspect ratio. We hypothesize that fibers may experience molecular stretching as tension is applied from the rotating collector. This phenomenon was minimized in the 24-hour cross-linking group, indicating that cross-linking limits swelling and contributes to the retention of scaffold architecture. However, these results reveal that near 100% cross-linking is needed for appreciable retention of scaffold dimensions to be measured. The same was not true when assessing tensile mechanical properties of the bulk scaffolds. Mechanical moduli increased as the degree of fiber alignment increased and as cross-linking density increased within fiber orientations. Mechanical properties have been shown to influence cell responses in skeletal muscle regeneration (*29*–*31*). As shown previously, native skeletal muscle has a tensile modulus of approximately 116 kPa (*19*), which was most closely mimicked in the AO 1000 group.

C2C12 myoblasts were used to assess the bioactivity of dECM and evaluate the effects of fiber alignment and cross-linking density on myotube formation. As anticipated, the degree of cross-linking affected cell attachment and subsequent growth (Fig. 4). By hindering cells' access to free amines and biochemical cues from the dECM substrate, fewer cells attached to the 24-hour cross-linked scaffolds compared to the uncross-linked and 30-min cross-linked samples. Similar trends were shown in protein scaffolds with varying degrees of cross-linking (*20*–*22*). The results further suggest that the 30-min cross-linked groups promoted growth at least as well as the uncross-linked counterparts, indicating that the combination of increased mechanical properties with access to biochemical stimuli from the dECM may help promote cell adhesion and growth. This is further supported in the uncross-linked groups, where increased cell growth was observed in the more highly aligned groups, which also had higher mechanical moduli. Other studies have, likewise, found that substrate stiffness affects cell behavior (*29*, *32*, *33*). The decreased response from the fully cross-linked groups also supports the hypothesis that bioactivity from the dECM substrate was preserved throughout processing. By day 4 of growth (Fig. 4), cells formed a confluent layer on all groups except the 24-hour cross-linked groups. Cell spreading and confluency are important to encourage cell fusion and myotube formation. Therefore, it is not unexpected that no myotube formation was observed in any of the 24-hour cross-linked groups. Without the biochemical cues provided by the dECM as assessed via free amines, the growth and differentiation cascades were considerably affected. We hypothesize that longer growth periods may support additional cell growth on the 24-hour cross-linked groups that would promote myotube formation (fig. S3).

Myotube formation was assessed through immunofluorescent imaging of desmin-positive myotubes after 7 days in induction media (Fig. 5). While the main influence for myotube alignment was fiber alignment, cross-linking allowed for further retention of scaffold architecture. These findings were concurrent with synthetic, aligned electrospun scaffolds guiding myotube alignment (*34*, *35*). AOX 3000 30 samples promoted the most aligned myotube formation, followed by AO 3000 and AOX 1000 30 samples. A similar trend was observed in assessing myotube length (Fig. 6). Myotube shape is an important metric because myofibers tend to be long and narrow. Fiber alignment and mechanical stimulation aided in promoting myotube elongation along the dECM fibers. Without structured architecture, myotubes grew in random orientations and less elongated. While function was not assessed under these culture conditions, it is hypothesized by the shape and orientation that greater force would be produced in more aligned and mechanically robust scaffolds. While the mechanism controlling myofiber fusion is not completely understood, studies have demonstrated that cell elongation enhances actomyosin contractility in myoblasts (*36*, *37*).

While we attempted to isolate the effects of cross-linking and fiber alignment on cell behavior, it is difficult to tease out the full impact of these parameters because mechanical properties are affected by both variables. In addition, the biochemical cues on the scaffold surface and those being released as degradation products from the dECM substrate cannot be overlooked. Scaffold degradation was observed in all groups except for the 24-hour cross-linked groups. The ability for cells to remodel the electrospun matrix may have contributed to increased differentiation. The most degraded scaffolds (AOX 3000 30 and AOX 1000 30) also contained the highest number of myotubes (Fig. 6). While retention of architecture is important to guide initial cell growth and alignment, later-stage degradation and release of ECM components may play a greater role in cell differentiation. Several studies have investigated dECM degradation products and found that they positively affect myogenic growth and differentiation (*38*–*40*). However, there is still much to be understood about the interplay of these mechanisms on myogenesis.

Overall, the work presented here demonstrated the tunability of bioactive electrospun dECM scaffolds and their ability to support cell growth and control myotube formation. Electrospinning overcomes the limitations of scalability of decellularized muscle, allowing the resulting dECM meshes to be scaled up to large clinical sizes only limited by the size of the electrospinning platforms, and many of these limitations have been reduced by the manufacturing of commercial electrospinning systems. While the use of electrospun scaffolds for skeletal muscle engineering is common, this is the first study, to our knowledge, that has used an electrospun scaffold completely derived from skeletal muscle dECM. The ability for the dECM substrate to guide myotube alignment was similar to that observed from synthetic polymers (*41*, *42*) and hybrids blended with ECM components (*35*), indicating that dECM is robust enough to provide physicochemical properties comparable to synthetic materials. We acknowledge the limitation of cell penetration into electrospun scaffolds that is not unique to our system. However, previous studies in our laboratory (*43*) and outside laboratories (*44*) have demonstrated that fluid flow drastically increases cell penetration within electrospun systems, providing promise for testing this system in vivo, where it will be exposed to stimuli such as fluid shear and mechanical stimulation. With few nonimaging-based analyses available for assessing myotube formation in vitro and a number of different culture conditions and cell types available, it can be difficult to compare results across studies. In particular, this study uses a less common myogenic marker, desmin, because of the nature of the dECM substrate. Myosin heavy chain (MHC) is a common myogenic marker because of its robust expression in differentiating C2C12 myoblasts. However, the dECM used in this study retains MHC, ruling it out as a cell marker. Another limitation of this study is the use of C2C12 myoblasts. While these precursor cells are easily grown, they have a very low differentiation percentage (*45*, *46*). Therefore, the results of the study may look more robust if a different cell type, such as primary satellite cells, was used. Last, we understand that imaging and analysis using an image processing software can lead to bias. While imaging and image analysis were attempted in a systematic way to limit bias, it is inherent with these types of techniques. Ultimately, we believe that the results presented here demonstrate that electrospun skeletal muscle dECM supports cell attachment, growth, and differentiation and that a bioactive dECM-based system with tunable physicochemical properties may bring the field of skeletal muscle engineering one step closer to developing a therapy to address unmet clinical needs.

MATERIALS AND METHODS

Decellularization of skeletal muscle tissue

Male New Zealand white rabbits were donated from Rice University in accordance with protocols approved by the Rice University Institutional Animal Care and Use Committee. Skeletal muscle tissue was harvested from the hind legs and was decellularized as described previously (*19*). The fascia and connective tissue were first removed; the tissue was then incubated in sterile ultrapure water containing 1% penicillin/streptomycin (P/S) (Sigma-Aldrich, St. Louis, MO) overnight at 4°C and under constant agitation. Tissue samples were then further cut and incubated in enzyme solution [0.025% trypsin (Sigma-Aldrich) and 0.05% EDTA (Sigma-Aldrich) in phosphate-buffered saline (PBS)] for 1 hour at room temperature. The tissue samples were then washed with PBS and incubated in 1% Triton X-100 (Sigma-Aldrich) containing 1% antibiotic overnight at 4°C and under constant agitation. After washing, the tissue was agitated in alternating hypotonic [10 mM tris-HCl (Sigma-Aldrich)] and hypertonic [50 mM tris-HCl and 1.5 M NaCl (Sigma-Aldrich)] salt solutions with 30-min incubations at room temperature. The samples were further cut if the tissue core remained colored after 2 cycles in each salt solution. After 3 cycles, the tissue was washed in ultrapure water for 24 hours to remove any remaining salt. The decellularized muscle (dECM) was then homogenized using a variable speed tissue homogenizer. Last, the slurry was frozen and dried.

Electrospinning dECM

dECM was electrospun as previously described (*19*). After drying, the dECM was ground into a fine powder and sieved to remove particles larger than 300 μm. Chilled hexafluoro-2-propanol (HFIP) (Oakwood Chemical, Estill, SC) was then added to dECM powder (10%, w/v) and stirred overnight at 4°C. To fabricate RO meshes, dECM/HFIP was electrospun onto a stationary plate at a flow rate of 1 ml/hour using a 22-gauge blunted needle. The collector carried a negative voltage of −2 kV and was placed approximately 15 cm away from the electrospinning needle, which carried a positive voltage of 7 kV. Electrospinning continued until the mesh reached the desired thickness, between 150 and 300 μm.

Aligned meshes were fabricated by electrospinning dECM/HFIP onto a rotating mandrel (Ø 8 cm). To electrospin the most aligned group (AO 3000), the dECM solution was extruded from a 22-gauge needle at a flow rate of 2 ml/hour. The fibers were collected on a grounded mandrel turning at 3000 ± 5 rpm located approximately 15 cm from the electrospinning needle, which carried a positive voltage of 13 kV. Likewise, to create meshes with an intermediate degree of fiber alignment, the mandrel was set to turn at 1000 ± 5 rpm. The extrusion rate and needle voltage were adjusted to 1.75 ml/hour and 12 kV, respectively, to create fibers with diameters similar to the RO and AO 3000 groups. Electrospinning continued until meshes reached the desired thickness. Upon completion, all meshes were dried, purged with nitrogen, and stored at 4°C until use.

For groups that required cross-linking, scaffolds were carefully placed inside a desiccator, ensuring that scaffolds did not overlap one another. Once GA (25%) was placed inside the desiccator, the system was sealed and placed under vacuum for the desired length of time.

Evaluation of degree of fiber alignment

The degree of fiber alignment was evaluated in all three groups of varying fiber orientation (RO, AO 1000, and AO 3000). Fluorescein was added to dECM electrospinning solutions to incorporate the fluorophore within single fibers. Samples were then imaged dry using a confocal microscope (Zeiss 5 Live). Areas imaged were randomly selected within five zones on the scaffold (center, upper right, upper left, lower right, and lower left) before examining the fibers to minimize bias. A z-stack was taken for each sample. The captured images were then processed in NIH ImageJ. An average intensity project was created by merging image slices within the z-stack. The directionality of the image was then evaluated via the Directionality plugin, with a total of 30 bins taken from −90° to 90°.

Evaluation of degree of cross-linking

The degree of cross-linking was correlated to the percentage of free amines within each dECM sample and measured via a ninhydrin

assay (*47*). After reacting with GA vapor for varying amounts of time (10 min to 24 hours), the electrospun dECM was weighed and then incubated in ultrapure water for 1 hour. Ninhydrin reagent solution (Sigma-Aldrich) was added to the samples and incubated for 5 min at 120°C. The solution was then cooled to room temperature and diluted with 95% ethanol. The optical absorbance of the solutions was measured at 570 nm using a plate reader (BioTek PowerWave, Winooski, VT). The degree of cross-linking was then calculated using the equation below

$$\text{Degree of cross} - \text{linking (\%)} = 100 - \text{Free amines (\%)}$$
$$= \left(1 - \frac{A_c}{A_u}\right) \times 100$$

A_c and A_u represent the absorbance values for the cross-linked and uncross-linked dECM, respectively.

Evaluation of fiber swelling

Fiber swelling was evaluated in all nine dECM groups as previously described using confocal microscopy (*19*). To measure dry fiber diameter, fluorescein was added to dECM electrospinning solutions. Stained scaffolds were then dried and imaged dry using a confocal microscope (Zeiss 5 Live). Areas imaged were randomly selected within the center of the scaffold before examining the fibers in those areas to minimize bias. NIH ImageJ was then used to evaluate each captured image. A line was drawn through the center of each image, and the fiber diameters of all fibers intersecting this line were measured. To measure swollen fiber diameter, scaffolds were submerged in PBS for 24 hours. Scaffolds were incubated in Nile red during the last 30 min of their swelling time and then imaged and evaluated in the same manner as the dry scaffolds.

Evaluation of bulk scaffold swelling

The bulk scaffold swelling of all nine dECM groups was evaluated as previously described (*19*). dECM scaffolds of approximately 8 mm in diameter were formed using a biopsy punch. The scaffold diameter was measured dry and after swelling in PBS for 24 hours. Dry scaffolds were placed between two microscope slides and positioned beside a standard ruler. The scaffolds were then imaged with a stereomicroscope. This process was repeated with swollen scaffolds. Images were then analyzed in NIH ImageJ image processing software. The boundaries of the scaffolds were defined, and the major and minor elliptical axis lengths were measured (see fig. S2). This process was further repeated on fixed scaffolds at 0, 2, 4, 7, 9, and 11 days in culture to assess in vitro degradation.

Mechanical testing of dECM scaffolds

The tensile mechanical properties of dECM groups were evaluated as previously described (*19*). A uniaxial tensile mechanical testing machine equipped with a room-temperature aqueous testing chamber was used to measure the tensile modulus of each dECM group. Electrospun dECM meshes were cut into 10 mm by 50 mm strips (0.2 ± 0.1 mm thickness). Aligned scaffolds were marked parallel to the fiber orientation, and the length (50 mm) was cut along the axis of alignment. The strips were then swollen in PBS before mechanical testing. Thickness and area were measured, and samples were loaded into the mechanical testing apparatus, with a gauge length of 30 mm set. Samples were pulled at a rate of 10% strain/min to an extension of 12 mm under aqueous conditions. The tensile modulus was then calculated for all samples. Surface area was incorporated into calculations for stress to normalize for changes in thickness across samples.

Cell seeding and culture on dECM scaffolds

C2C12 mouse myoblasts [American Type Culture Collection (ATCC), Manassas, VA] were cultured in growth media containing Dulbecco's modified Eagle's media (DMEM) supplemented with 10% fetal bovine serum (ATCC) and 1% P/S at 37°C in a humidified 5% CO_2 atmosphere. The cells were used for experiments at passage 5. A 10-mm biopsy punch was used to shape scaffolds for cell culture. Scaffolds were ultraviolet-sterilized for 30 min on each side. All further steps were performed under sterile conditions. Scaffolds cross-linked with GA were incubated overnight in 0.1 M glycine solution and then washed twice. All groups were then incubated overnight in PBS. Scaffolds and myoblasts were combined in a 20-ml syringe at a concentration of 1×10^5 cells/ml per scaffold. Excess air was removed from the syringe and capped with a 0.2-μm polyethersulfone membrane syringe filter to create a sterile, compressed system. Cells were allowed to attach to electrospun scaffolds overnight while rotating (15 rpm) in an incubator (37°C, 5% CO_2). After seeding, composites were placed into nontreated 48-well plates and allowed to grow for 4 days. Samples reserved for growth analysis were removed from culture and fixed with 4% paraformaldehyde (PFA) at days 2 and 4 of this growth period. Induction media (DMEM, 2% horse serum, and 1% P/S) was then added to the remaining groups. Myoblasts were allowed to differentiate for 7 days with media changes as needed or every 3 days. Upon completion of the study, scaffolds were fixed with 4% PFA for 10 min, washed three times, and stored in PBS at 4°C until use.

Immunofluorescence staining and morphological analysis

After 2 and 4 days in culture, cell-seeded dECM constructs were fixed with 4% PFA, washed three times with PBS, and stained with Hoechst 33342 solution (1:1000 dilution; Invitrogen, Carlsbad, CA) and Phalloidin-iFluor 488 (1:1000 dilution; Abcam, Cambridge, MA) to visualize nuclei and actin cytoskeletons, respectively. Stains were diluted in antibody buffer (1% bovine serum albumin, 0.3% Triton X-100, and PBS). After incubating fixed constructs for 1 hour at room temperature, scaffolds were washed three times with PBS and incubated in TrueVIEW (Vector Laboratories, Burlingame, CA) for 5 min to reduce scaffold fluorescence. Samples were then imaged via confocal microscopy. Areas imaged were randomly selected within three zones on the scaffold to minimize bias. Captured images were then analyzed through NIH ImageJ software to measure the total number of nuclei and cell confluency. These values were used as metrics for cell growth for each of the dECM groups.

After differentiating for 7 days in induction media, cell-laden dECM constructs were fixed with 4% PFA, washed three times with PBS, and stained to assess myotube formation. Samples were incubated in mouse anti-desmin primary antibody (1:200; Santa Cruz Biotechnology) overnight at 4°C. Samples were then washed three times and incubated in Alexa Fluor 488 secondary antibody (1:200; Santa Cruz Biotechnology, Dallas, TX), Phalloidin-iFluor 594 (1:1000 dilution; Abcam), and Hoechst (1:1000) for 1 hour. After incubation, scaffolds were washed three times with PBS and incubated in TrueVIEW for 5 min to reduce scaffold fluorescence. Samples were then imaged via confocal microscopy (Nikon A1). Immunocytochemistry controls were performed to ensure that desmin antibody labeled

differentiating myotubes (fig. S4). Areas imaged were randomly selected within three zones on the scaffold to minimize bias. Captured images were then analyzed through Photoshop to measure the fusion index, length, width, and alignment of desmin-positive myotubes that met the following criteria: (i) must have three or more nuclei; (ii) must express desmin; and (iii) multinucleated structures satisfying the first two criteria that are joined by any cytoplasmic process are considered to be a single myotube. Myotube analysis in Photoshop was performed systematically as described elsewhere (*48*).

Statistics

All data are expressed as means ± SD. The number of replicates used for each analysis is stated in Results above. Statistical significance for all analyses was determined using a one-way analysis of variance (ANOVA) test paired with post hoc analysis by Tukey's post hoc test. A significance level of $P < 0.05$ was used.

There remains a great need for innovative tissue-engineered therapies that can promote regrowth of functional muscle following VML defects. Leveraging electrospinning with skeletal muscle dECM allows for the fabrication of biochemical-rich scaffolds with tunable physicochemical properties. By modulating cross-linking density and degree of fiber alignment within dECM scaffolds, we have identified physical and biochemical properties that are necessary for myotube formation. While intermediate cross-linking provided mechanical properties that promoted cell attachment, 100% cross-linking hindered cell attachment and growth by restricting access to free amines needed to support these functions and biochemical cues from the dECM substrate necessary to facilitate growth and myotube formation. Our studies also support the hypothesis that fiber alignment can provide the necessary framework to guide myoblast and myotube alignment. Myotube formation and subsequent growth and alignment were controlled by modulation of material properties and scaffold architecture. Through the use of bioinspired tissue-engineered scaffolds that control muscle formation, the field of skeletal muscle engineering may be one step closer to achieving a therapy for skeletal muscle reconstruction and functional repair.

SUPPLEMENTARY MATERIALS

Supplementary material for this article is available at http://advances.sciencemag.org/cgi/content/full/7/20/eabg4123/DC1

View/request a protocol for this paper from *Bio-protocol*.

REFERENCES AND NOTES

1. C. J. Mann, E. Perdiguero, Y. Kharraz, S. Aguilar, P. Pessina, A. L. Serrano, P. Muñoz-Cánoves, Aberrant repair and fibrosis development in skeletal muscle. *Skelet. Muscle.* **1**, 21 (2011).
2. M. A. A. Mahdy, Skeletal muscle fibrosis: An overview. *Cell Tissue Res.* **375**, 575–588 (2019).
3. J. M. Grasman, M. J. Zayas, R. L. Page, G. D. Pins, Biomimetic scaffolds for regeneration of volumetric muscle loss in skeletal muscle injuries. *Acta Biomater.* **25**, 2–15 (2015).
4. K. Garg, C. L. Ward, C. R. Rathbone, B. T. Corona, Transplantation of devitalized muscle scaffolds is insufficient for appreciable de novo muscle fiber regeneration after volumetric muscle loss injury. *Cell Tissue Res.* **358**, 857–873 (2014).
5. J. Dziki, S. Badylak, M. Yabroudi, B. Sicari, F. Ambrosio, K. Stearns, N. Turner, A. Wyse, M. L. Boninger, E. H. P. Brown, J. P. Rubin, An acellular biologic scaffold treatment for volumetric muscle loss: Results of a 13-patient cohort study. *NPJ Regen. Med.* **1**, 16008 (2016).
6. S. M. Greising, C. L. Dearth, B. T. Corona, Regenerative and rehabilitative medicine: A necessary synergy for functional recovery from volumetric muscle loss injury. *Cells Tissues Organs* **202**, 237–249 (2016).
7. B. M. Sicari, J. P. Rubin, C. L. Dearth, M. T. Wolf, F. Ambrosio, M. Boninger, N. J. Turner, D. J. Weber, T. W. Simpson, A. Wyse, E. H. P. Brown, J. L. Dziki, L. E. Fisher, S. Brown, S. F. Badylak, An acellular biologic scaffold promotes skeletal muscle formation in mice and humans with volumetric muscle loss. *Sci. Transl. Med.* **6**, 234ra58 (2014).
8. J. A. Passipieri, H. B. Baker, M. Siriwardane, M. D. Ellenburg, M. Vadhavkar, J. M. Saul, S. Tomblyn, L. Burnett, G. J. Christ, Keratin hydrogel enhances in vivo skeletal muscle function in a rat model of volumetric muscle loss. *Tissue Eng. Part A.* **23**, 556–571 (2017).
9. P. Lazarovici, C. Marcinkiewicz, P. I. Lelkes, Cross talk between the cardiovascular and nervous systems: Neurotrophic effects of vascular endothelial growth factor (VEGF) and angiogenic effects of nerve growth factor (NGF)-implications in drug development. *Curr. Pharm. Des.* **12**, 2609–2622 (2006).
10. N. Kikuno, K. Kawamoto, H. Hirata, K. Vejdani, K. Kawakami, T. Fandel, L. Nunes, S. Urakami, H. Shiina, M. Igawa, E. Tanagho, R. Dahiya, Nerve growth factor combined with vascular endothelial growth factor enhances regeneration of bladder acellular matrix graft in spinal cord injury-induced neurogenic rat bladder. *BJU Int.* **103**, 1424–1428 (2009).
11. B. Nico, D. Mangieri, V. Benagiano, E. Crivellato, D. Ribatti, Nerve growth factor as an angiogenic factor. *Microvasc. Res.***75**, 135–141 (2008).
12. M. M. Smoak, A. G. Mikos, Advances in biomaterials for skeletal muscle engineering and obstacles still to overcome. *Mater. Today Bio.* **7**, 100069 (2020).
13. R. Augustine, P. Dan, A. Sosnik, N. Kalarikkal, N. Tran, B. Vincent, S. Thomas, P. Menu, D. Rouxel, Electrospun poly(vinylidene fluoride-trifluoroethylene)/zinc oxide nanocomposite tissue engineering scaffolds with enhanced cell adhesion and blood vessel formation. *Nano Res.* **10**, 3358–3376 (2017).
14. J. Gilbert-Honick, S. R. Iyer, S. M. Somers, R. M. Lovering, K. Wagner, H. Q. Mao, W. L. Grayson, Engineering functional and histological regeneration of vascularized skeletal muscle. *Biomaterials* **164**, 70–79 (2018).
15. N. Bloise, E. Berardi, C. Gualandi, E. Zaghi, M. Gigli, R. Duelen, G. Ceccarelli, E. Cortesi, D. Costamagna, G. Bruni, N. Lotti, M. Focarete, L. Visai, M. Sampaolesi, Ether-oxygen containing electrospun microfibrous and sub-microfibrous scaffolds based on poly(butylene 1,4-cyclohexanedicarboxylate) for skeletal muscle tissue engineering. *Int. J. Mol. Sci.* **19**, 3212 (2018).
16. N. Narayanan, C. Jiang, C. Wang, G. Uzunalli, N. Whittern, D. Chen, O. G. Jones, S. Kuang, M. Deng, Harnessing fiber diameter-dependent effects of myoblasts toward biomimetic scaffold-based skeletal muscle regeneration. *Front. Bioeng. Biotechnol.* **8**, 203 (2020).
17. Y. Liu, G. Zhou, Z. Liu, M. Guo, X. Jiang, M. B. Taskin, Z. Zhang, J. Liu, J. Tang, R. Bai, F. Besenbacher, M. Chen, C. Chen, Mussel inspired polynorepinephrine functionalized electrospun polycaprolactone microfibers for muscle regeneration. *Sci. Rep.* **7**, 1–10 (2017).
18. S. Manchineella, G. Thrivikraman, K. K. Khanum, P. C. Ramamurthy, B. Basu, T. Govindaraju, Pigmented silk nanofibrous composite for skeletal muscle tissue engineering. *Adv. Healthc. Mater.* **5**, 1222–1232 (2016).
19. M. M. Smoak, A. Han, E. Watson, A. Kishan, K. J. Grande-Allen, E. Cosgriff-Hernandez, A. G. Mikos, Fabrication and characterization of electrospun decellularized muscle-derived scaffolds. *Tissue Eng. C Methods* **25**, 276–287 (2019).
20. C. N. Grover, J. H. Gwynne, N. Pugh, S. Hamaia, R. W. Farndale, S. M. Best, R. E. Cameron, Crosslinking and composition influence the surface properties, mechanical stiffness and cell reactivity of collagen-based films. *Acta Biomater.* **8**, 3080–3090 (2012).
21. D. V. Bax, N. Davidenko, D. Gullberg, S. W. Hamaia, R. W. Farndale, S. M. Best, R. E. Cameron, Fundamental insight into the effect of carbodiimide crosslinking on cellular recognition of collagen-based scaffolds. *Acta Biomater.* **49**, 218–234 (2017).
22. X. Jiang, G. T. Christopherson, H.-Q. Mao, The effect of nanofibre surface amine density and conjugate structure on the adhesion and proliferation of human haematopoietic progenitor cells. *Interface Focus* **6**, 725–733 (2011).
23. T. Pan, J. Tao, Q. Meng, W. Zhao, B. Song, S. Qi, Importance of the free amine groups in acellular scaffold during tissue repairing or regeneration process. *J. Biomater. Appl.* **34**, 25–35 (2019).
24. I. Vlodavsky, J. Folkman, R. Sullivan, R. Fridman, R. Ishai-Michaeli, J. Sasse, M. Klagsbrun, Endothelial cell-derived basic fibroblast growth factor: Synthesis and deposition into subendothelial extracellular matrix. *Proc. Natl. Acad. Sci. U.S.A.* **84**, 2292–2296 (1987).
25. I. Vlodavsky, H.-Q. Miao, B. Medalion, P. Danagher, D. Ron, Involvement of heparan sulfate and related molecules in sequestration and growth promoting activity of fibroblast growth factor. *Cancer Metastasis Rev.* **15**, 177–186 (1996).
26. K. H. Patel, M. Talovic, A. J. Dunn, A. Patel, S. Vendrell, M. Schwartz, K. Garg, Aligned nanofibers of decellularized muscle extracellular matrix for volumetric muscle loss. *J. Biomed. Mater. Res. B Appl. Biomater.* **108**, 2528–2537 (2020).
27. A. W. Martinez, J. M. Caves, S. Ravi, W. Li, E. L. Chaikof, Effects of crosslinking on the mechanical properties, drug release and cytocompatibility of protein polymers. *Acta Biomater.* **10**, 26–33 (2014).
28. S. R. Gomes, G. Rodrigues, G. G. Martins, C. M. R. Henriques, J. C. Silva, In vitro evaluation of crosslinked electrospun fish gelatin scaffolds. *Mater. Sci. Eng. C* **33**, 1219–1227 (2013).

29. M. M. Smoak, H. A. Pearce, A. G. Mikos, Microfluidic devices for disease modeling in muscle tissue. *Biomaterials* **198**, 250–258 (2019).
30. C. A. Powell, B. L. Smiley, J. Mills, H. H. Vandenburgh, Mechanical stimulation improves tissue-engineered human skeletal muscle. *Am. J. Physiol. Cell Physiol.* **283**, 1557–1565 (2002).
31. A. Rainer, C. Gargioli, S. Maria Giannitelli, C. Escobedo-Lucea, B. Maleiner, J. Tomasch, P. Heher, O. Spadiut, D. Rünzler, C. Fuchs, The importance of biophysical and biochemical stimuli in dynamic skeletal muscle models. *Front. Physiol.* **1**, 1130 (2018).
32. D. E. Discher, P. Janmey, Y.-L. Wang, Tissue cells feel and respond to the stiffness of their substrate. *Science* **310**, 1139–1143 (2005).
33. S. Romanazzo, G. Forte, M. Ebara, K. Uto, S. Pagliari, T. Aoyagi, E. Traversa, A. Taniguchi, Substrate stiffness affects skeletal myoblast differentiation in vitro. *Sci. Technol. Adv. Mater.* **13**, 064211 (2012).
34. K. J. Aviss, J. E. Gough, S. Downes, Aligned electrospun polymer fibres for skeletal muscle regeneration. *Eur. Cells Mater.* **19**, 193–204 (2010).
35. J. S. Choi, S. J. Lee, G. J. Christ, A. Atala, J. J. Yoo, The influence of electrospun aligned poly(ε-caprolactone)/collagen nanofiber meshes on the formation of self-aligned skeletal muscle myotubes. *Biomaterials* **29**, 2899–2906 (2008).
36. C. Bruyère, M. Versaevel, D. Mohammed, L. Alaimo, M. Luciano, E. Vercruysse, S. Gabriele, Actomyosin contractility scales with myoblast elongation and enhances differentiation through YAP nuclear export. *Sci. Rep.* **9**, 15565 (2019).
37. A. N. Johnson, M. H. Mokalled, J. M. Valera, K. D. Poss, E. N. Olson, Post-transcriptional regulation of myotube elongation and myogenesis by Hoi polloi. *Development* **140**, 3645–3656 (2013).
38. L. Huleihel, J. L. Dziki, J. G. Bartolacci, T. Rausch, M. E. Scarritt, M. C. Cramer, T. Vorobyov, S. T. LoPresti, I. T. Swineheart, L. J. White, B. N. Brown, S. F. Badylak, Macrophage phenotype in response to ECM bioscaffolds. *Semin. Immunol.* **29**, 2–13 (2017).
39. J. L. Dziki, L. Huleihel, M. E. Scarritt, S. F. Badylak, Extracellular matrix bioscaffolds as immunomodulatory biomaterials. *Tissue Eng. A* **23**, 1152–1159 (2017).
40. J. E. Reing, L. Zhang, J. Myers-Irvin, K. E. Cordero, D. O. Freytes, E. Heber-Katz, K. Bedelbaeva, D. McIntosh, A. Dewilde, S. J. Braunhut, S. F. Badylak, Degradation products of extracellular matrix affect cell migration and proliferation. *Tissue Eng. A* **15**, 605–614 (2009).
41. N. F. Huang, S. Patel, R. G. Thakar, J. Wu, B. S. Hsiao, B. Chu, R. J. Lee, S. Li, Myotube assembly on nanofibrous and micropatterned polymers. *Nano Lett.* **6**, 537–542 (2006).
42. L. Ricotti, A. Polini, G. G. Genchi, G. Ciofani, D. Iandolo, H. Vazão, V. Mattoli, L. Ferreira, A. Menciassi, D. Pisignano, Proliferation and skeletal myotube formation capability of C2C12 and H9c2 cells on isotropic and anisotropic electrospun nanofibrous PHB scaffolds. *Biomed. Mater.* **7**, 035010 (2012).
43. Q. P. Pham, U. Sharma, A. G. Mikos, Electrospun poly(ε-caprolactone) microfiber and multilayer nanofiber/microfiber scaffolds: Characterization of scaffolds and measurement of cellular infiltration. *Biomacromolecules* **7**, 2796–2805 (2006).
44. N. L. Nerurkar, S. Sen, B. M. Baker, D. M. Elliott, R. L. Mauck, Dynamic culture enhances stem cell infiltration and modulates extracellular matrix production on aligned electrospun nanofibrous scaffolds. *Acta Biomater.* **7**, 485–491 (2011).
45. T. Miyake, J. C. McDermott, A. O. Gramolini, A method for the direct identification of differentiating muscle cells by a fluorescent mitochondrial dye. *PLOS ONE* **6**, e28628 (2011).
46. C. Schöneich, E. Dremina, N. Galeva, V. Sharov, Apoptosis in differentiating C2C12 muscle cells selectively targets Bcl-2-deficient myotubes. *Apoptosis* **19**, 42–57 (2014).
47. A. P. Kishan, R. M. Nezarati, C. M. Radzicki, A. L. Renfro, J. L. Robinson, M. E. Whitely, E. M. Cosgriff-Hernandez, In situ crosslinking of electrospun gelatin for improved fiber morphology retention and tunable degradation. *J. Mater. Chem. B* **3**, 7930–7938 (2015).
48. C. C. Agley, C. P. Velloso, N. R. Lazarus, S. D. R. Harridge, An image analysis method for the precise selection and quantitation of fluorescently labeled cellular constituents: Application to the measurement of human muscle cells in culture. *J. Histochem. Cytochem.* **60**, 428–438 (2012).

Acknowledgments: We would like to thank A. Han in the laboratory of A.G.M. and C. Sylvester and S. Mehta in the laboratory of K.J.G.-A. for assistance. **Funding:** We acknowledge support toward the development of dECM scaffolds from the NIH (P41 EB023833). We also acknowledge support from an NSF Graduate Research Fellowship (to M.M.S.), a Ford Foundation Pre-doctoral Research Fellowship (to M.M.S.), and the National Institute of Dental and Craniofacial Research (F31 DE030333, to K.J.H.). **Author contributions:** M.M.S., K.J.H., and A.G.M. planned the experiments and oversaw the utilization of the study. M.M.S. and K.J.H. fabricated the materials used in the studies. M.M.S. performed the experiments. M.M.S., K.J.H., K.J.G.-A., and A.G.M. participated in the discussion of the data and analysis. M.M.S. wrote the manuscript, and K.J.H., K.J.G.-A., and A.G.M. participated in editing and revising the manuscript. **Competing interests:** The authors declare that they have no competing interests. **Data and materials availability:** All data needed to evaluate the conclusions in the paper are present in the paper and/or the Supplementary Materials. Additional data related to this paper may be requested from the authors.

Submitted 4 January 2021
Accepted 25 March 2021
Published 14 May 2021
10.1126/sciadv.abg4123

Citation: M. M. Smoak, K. J. Hogan, K. J. Grande-Allen, A. G. Mikos, Bioinspired electrospun dECM scaffolds guide cell growth and control the formation of myotubes. *Sci. Adv.* **7**, eabg4123 (2021).